# 11. TAG-5 AREA[1]

Shipboard Scientific Party[2]

## HOLE 957O

**Date occupied:** 13 November 1994

**Date departed:** 14 November 1994

**Time on hole:** 1 day, 45 min

**Position:** 26°8.241′N, 44°49.575′W

**Bottom felt (drill-pipe measurement from rig floor, m):** 3648.0

**Distance between rig floor and sea level (m):** 11.87

**Water depth (drill-pipe measurement from sea level, m):** 3636.13

**Total depth (from rig floor, m):** 3668.5

**Penetration (m):** 20.5

**Number of cores (including cores having no recovery):** 4

**Total length of cored section (m):** 20.5

**Total core recovered (m):** 1.27

**Core recovery (%):** 6.2

**Hard rock:**
Depth (mbsf): 20.5
Nature: Pyrite and pyrite-anhydrite breccias

## HOLE 957P

**Date occupied:** 14 November 1994

**Date departed:** 15 November 1994

**Time on hole:** 1 day, 12 hr, 15 min

**Position:** 26°8.236′N, 44°49.558′W

**Bottom felt (drill-pipe measurement from rig floor, m):** 3648.0

**Distance between rig floor and sea level (m):** 11.87

**Water depth (drill-pipe measurement from sea level, m):** 3636.13

**Total depth (from rig floor, m):** 3707.4

**Penetration (m):** 59.4

**Number of cores (including cores having no recovery):** 13

**Total length of cored section (m):** 59.4

**Total core recovered (m):** 4.62

**Core recovery (%):** 57.8

**Hard rock:**
Depth (mbsf): 59.4
Nature: Pyrite, pyrite-anhydrite, and pyrite-silica breccias

**Comments:** Core 158-957P-13W was a wash core recovered from previously drilled interval (15.0–39.0 mbsf).

**Principal results:** Holes 957O and 957P are about 15 m apart and are located near the margin of the upper terrace on the north side of the mound about 20–30 m north-northeast of the Black Smoker Complex (this area is designated as TAG-5). The objectives of drilling at this location were to determine the lateral heterogeneity of the sulfide mineralization and to delineate the northern extent of the underlying stockwork zone. The upper part of the section from 0 to 20.5 mbsf was cored at Hole 957O, although material was recovered only from 7.9 to 20.5 mbsf. The overall recovery for the entire 20.5 m section was 6.2%; however, between 7.9 and 20.5 m, recovery of 10.1% was achieved. Hole 957P is located 15 m west of Hole 957O; it was cored from 0 to 59.4 mbsf with recovery of 12%.

The overall stratigraphy inferred from core recovered from Holes 957O and 957P is similar to that observed in Holes 957C, 957E, 957F, and 957G in the TAG-1 area to the east of the Black Smoker Complex. Massive pyrite and semi-massive pyrite-anhydrite breccias comprise the dominant lithology from the surface down to a depth of about 10 mbsf, below which there is a 20-m-thick zone of massive granular and brecciated pyrite and massive pyrite-anhydrite breccias. Between 30 and 45 mbsf, this zone grades into pyrite-silica breccias, which contain fragments of silicified basalt and extend down to about 55 m. Silicified wallrock breccias comprise the lower part of the cored section. The last two cores from Hole 957P consisted of sand-sized fragments of pyrite, quartz, anhydrite, and Fe-oxide that represent drill cuttings. Embedded within them are large fragments of massive granular pyrite, pyrite-silica breccia, and silicified wallrock breccia.

The upper part of the section is comprised dominantly of nodular pyrite and pyrite-anhydrite breccia, similar to those in the anhydrite-rich zone in the TAG-1 area. The hard, cherty layer encountered in the upper few meters in the other areas (TAG-2, TAG-3, and TAG-4) was not recovered at TAG-5. Nodular pyrite breccias are composed of nodular pyrite clasts and angular aggregates about 1 cm in diameter in a matrix of fine sandy pyrite and anhydrite (up to 20 vol%). Geochemical analyses indicate S and Fe concentrations of 45.1 and 33.0 wt%, respectively. The Cu content is high (3.7 wt%), but the Zn content is low (0.03 wt%). The analyzed sample contains 4.5 ppm Ag, but concentrations of Cd were below the detection limit. The Fe, Zn, Cu, and S contents are within the range of similar samples taken from the TAG-1 and TAG-2 areas. The pyrite-anhydrite breccias contain nodular to angular clasts of pyrite (as large as 2 cm in diameter) and smaller (<3 mm in diameter) aggregates of chalcopyrite in a matrix of fine- to medium-grained pyrite and anhydrite. Anhydrite comprises up to 60 vol% of the rock and occurs in vugs, as irregular veins, and as matrix.

The proportion of anhydrite and vein-related mineralization increases below 10 mbsf. Vein-related pyrite-anhydrite breccias have a banded texture and are characterized by fine- to coarse-grained pyrite and chalcopyrite disseminated in anhydrite. Massive granular pyrite is also present and is associated with the anhydrite veining and pyrite-anhydrite breccias; it consists of pyrite as granular or crustiform banded aggregates and intergrown with chalcopyrite.

Below 30 mbsf, massive, coarse-grained granular pyrite is associated with the pyrite-silica breccias and contains significant amounts of silica.

[1]Humphris, S.E., Herzig, P.M., Miller, D.J., et al., 1996. *Proc. ODP, Init. Repts.*, 158: College Station, TX (Ocean Drilling Program).

[2]Shipboard Scientific Party is as given in the list of participants in the contents.

Remnant patches of chert, dark gray silica, and silicified altered basalt material are commonly included within the massive pyrite, suggesting that the rock formed by pyritization of an existing pyrite-silica or silicified wallrock breccia. The pyrite-silica breccia consists of coarse, poorly sorted pyrite aggregates in a matrix of fine-grained dark gray silica with coarse disseminated pyrite. Anhydrite is common, but it is confined to vugs and late veining. These breccias contain clasts of an earlier generation of pale-gray, fine-grained pyrite-silica breccia, indicating that there have been at least two stages of brecciation.

In Hole 957P, 1 mm to 5 cm, round to angular to irregularly shaped clasts of silicified wallrock occur in pyrite-silica breccias from 35 mbsf to the bottom of the core at 59.4 mbsf. The clasts are replaced by quartz, gray chlorite(?), and 0.1–1 mm pyrite grains and aggregates; they commonly have 0.5–3 mm rims of pyrite. Many of the clasts are intensively pyritized. The matrix is white to dark gray quartz + pyrite. Silicified basalt clasts are also common in massive pyrite matrix at depths greater than 45 mbsf in Hole 957P. These basalt clasts are more intensively replaced by pyrite than those in the pyrite-silica breccias.

The breccias and massive pyrite containing silicified basalt clasts in Hole 957P contain numerous veins, indicating multiple stages of veining, brecciation, and cementation. This sequence is generally similar to that in the other cores from the TAG mound and presents clear evidence for at least two stages of brecciation and cementation in cores from Hole 957P. The first veins to form in the basalt clasts were early, thin (0.1–1 mm), pyrite veins. These are cut by 1–3 mm quartz + pyrite veins and are reopened by 1–3 mm white quartz veins. The breccia matrix, which consists of white quartz plus 0.1–1 mm grains and aggregates of pyrite, cuts earlier quartz + pyrite veins. Clasts of basalt with this white quartz + pyrite matrix were rebrecciated, rimmed by a 1–3 mm layer of pyrite, and then cemented by a later dark gray quartz + pyrite matrix. This later dark gray quartz + pyrite matrix is cut by 0.1–1 mm vuggy pyrite veins, and by 0.5–1 cm massive pyrite veins, with late chalcopyrite in open spaces of the pyrite veins. Finally, anhydrite occurs on the outer, broken surfaces of many pieces and fills pore spaces in pyrite veins.

An important observation in core samples recovered from Holes 957O and 957P is the presence of fine (0.5 mm) grains of euhedral hexagonal pyrrhotite in two samples. Pyrrhotite occurs intergrown with anhydrite in a late anhydrite vein that coats the surface of a piece of nodular pyrite breccia recovered from a depth of less than 10.9 mbsf in Hole 957O. In addition, it occurs as a late phase overgrowing pyrite and filling interstices in a piece of porous massive pyrite recovered between 35.1 and 40.1 mbsf in Hole 957P. The only other reported occurrences of pyrrhotite in samples from the active TAG mound are as rare 5–10 μm anhedral inclusions in pyrite in two samples recovered from Hole 957E in the TAG-1 area, and as very fine (30 μm) euhedral grains in a sulfide crust sample from the surface of the mound at the Black Smoker Complex. In all cases, pyrrhotite is present in only trace amounts.

Physical properties measurements were made on 11 sulfide samples from Holes 957O and 957P. Bulk densities range from 3.37 to 5.19 g/cm$^3$ and porosities from 3.8% to 11.2%, similar to the values measured on samples from the TAG-1 and TAG-2 areas. Electrical resistivities measured on two sulfide minicores are low (0.13 and 0.19 Ωm) and show the same inverse relationship to porosity as found in samples from the TAG-1 and TAG-2 areas. Compressional (*P*-wave) velocities measured on the same minicores are 5.4 and 5.8 km/s. Thermal conductivities measured on half-round slabs are relatively high (10.2 and 10.5 W/[m·K]) and comparable to similar measurements made on cores from the eastern side of the mound in the TAG-1 and TAG-2 areas.

Paleomagnetic measurements were completed on two pyrite-rich samples from Hole 957O. The NRM intensities of these two samples are comparable with those of samples recovered from TAG-1 and TAG-2 areas, although the Koenigsberger ratios and the initial magnetic susceptibilities are higher. The anisotropy of magnetic susceptibility (AMS) is similar to those of samples recovered from the TAG-1 and TAG-2 areas, as well as to the basalt samples from the TAG-4 area, suggesting that no significant magnetic anisotropy exists in these samples. Vertically directed, drilling-induced magnetization could be removed relative easily from the nodular pyrite breccia by AF demagnetization. However, AF demagnetization was not sufficient to completely remove this overprint from the pyrite-anhydrite breccia. Similar examples of this behavior were also seen in samples from other TAG areas, and the more heavily overprinted samples are often associated with the presence of anhydrite and also come from relatively deeper sections in the mound. This suggests that the hydrothermal processes that have produced the entire TAG mound may have resulted in distinct zones where precipitates have their own characteristic magnetic properties. These zones are likely to reflect different mineralogical and chemical compositions and hence variable ability to acquire and maintain magnetic overprints.

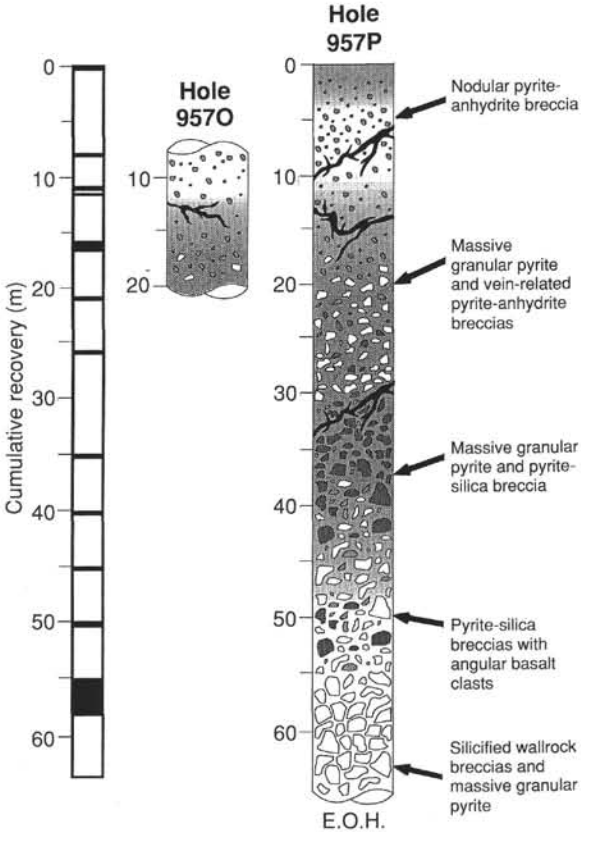


Figure 1. Schematic stratigraphic section of the mound in the TAG-5 area showing the distribution of the principal rock types in cores from Holes 957O and 957P. E.O.H. = end of hole.

## STRATIGRAPHY

### Introduction

Holes 957O and 957P, in the TAG-5 area, are located near the margin of the upper terrace on the north side of the mound. The holes are about 15 m apart and located 20–30 m northeast of the Black Smoker Complex. A portion of the upper part of the section was cored in Hole 957O from 0 to 20.5 mbsf, with a recovery of 6.2%, although core material was retrieved only between 8 and 20.5 m. Hole 957P was drilled from a seafloor depth of 3649 m and penetrated to a maximum depth of 59 mbsf. The core from Hole 957P contains a stratigraphic section from 0 to 59.4 mbsf, with a recovery of 12%. Graphic logs of the most complete core sections are shown in Figure 1, and Table 1 lists the different rock types and their distribution in each core. For more detailed descriptions of the rock types encountered in the TAG-5 area, see the "Sulfide Petrology and Geochemistry" section (this chapter).

**Table 1. Distribution of dominant lithologies in core from the TAG-5 area.**

| Dominant lithology | Intervals recovered | | Approximate location: Top (mbsf) | Approximate location: Bottom (mbsf) | Estimated total thickness (m) |
|---|---|---|---|---|---|
| Porous, massive pyrite (Type 5) and nodular pyrite-anhydrite breccia (Type 7) | 158-957P-1R-1 | (0–0.7 m) | 0 | 0.7 | 10 |
| | 158-967P-2R-1 | (0–0.1 m) | 7.9 | 8.0 | |
| | 158-957O-2R-1 | (0–0.4 m) | 7.9 | 8.3 | |
| | 158-957O-3R-1 | (0–0.3 m) | 10.9 | 11.2 | |
| Massive, granular pyrite (Type 5) ± vein-related pyrite-anhydrite breccia (Type 7) | 158-957P-3R-1 | (0–0.1 m) | 11.9 | 12.0 | 20 |
| | 158-957P-4R-1 | (0–0.1 m) | 16.9 | 17.0 | |
| | 158-957P-5R-1 | (0–0.1 m) | 21.5 | 21.6 | |
| | 158-957P-6R-1 | (0–0.3 m) | 26.5 | 26.8 | |
| | 158-957O-4R-1 | (0–0.9 m) | 15.9 | 16.8 | |
| Massive, granular pyrite (Type 5) and pyrite-silica breccias (Type 9) | 158-957P-7R-1 | (0–0.1 m) | 35.1 | 35.2 | 15 |
| | 158-957P-8R-1 | (0–0.3 m) | 35.1 | 35.4 | |
| | 158-957P-9R-1 | (0–0.3 m) | 40.1 | 40.4 | |
| | 158-957P-10R-1 | (0–0.3 m) | 45.1 | 45.4 | |
| Pyrite-silica breccias (Type 9) with angular basalt clasts | 158-957P-11R-1 | (0–0.6 m) | 50.1 | 50.7 | 12 |
| | 158-957P-12R-2 | (0–0.7 m) | 55.6 | 56.7 | |
| | 158-957P-12R-3 | (0–0.8 m) | 56.3 | 57.1 | |
| Silicified wallrock breccias (Type 10a) ± massive granular pyrite | 158-957P-12R-4 | (0–0.9 m) | 57.1 | 58.0 | — |

## Distribution of Lithologies

Although recoveries were low, the rocks recovered suggest that the sulfide stratigraphy in Holes 957O and 957P is similar to that in the TAG-1 area, 40 m to the south. From the surface to a depth of about 10 mbsf, the mound consists of semi-massive and massive pyrite-anhydrite breccias on top of a 20-m-thick zone of massive brecciated pyrite and vein-related, pyrite-anhydrite breccias. The massive pyrite-anhydrite zone grades downsection into pyrite-silica breccias between 35 and 45 mbsf and is underlain by pyrite-silica breccias and siliceous wallrock breccias from 45 mbsf to the maximum depth cored. The anhydrite-rich portion of the section is constrained to a narrow zone between 5 and 15 mbsf, and is somewhat more restricted than in the TAG-1 area. In addition, the massive and semi-massive pyrite appears to be much more abundant in the TAG-5 area than at TAG-1, although this may be an artifact of poor recovery. Pyrite-silica breccias and silicified wallrock breccias are the dominant lithologies in the lower 30 m of core and probably represent part of the quartz-rich stockwork.

The first few meters of core from the upper part of the mound contain mainly nodular pyrite-anhydrite breccias, similar to those in the anhydrite-rich zone in the TAG-1 area. The hard, cherty material and massive pyrite breccias encountered on top of this zone in the TAG-2, TAG-3, and TAG-4 areas were not recovered. Anhydrite is most abundant above 10 to 15 mbsf, but it also occurs as veins in massive pyrite-anhydrite breccias to a depth of about 25 mbsf. Nodular pyrite clasts or aggregates and massive to semi-massive pyrite account for 50 to 90 vol% of the rock in the anhydrite-rich zone. The pyrite-anhydrite breccias appear to grade downsection into dominantly vein-related, pyrite breccias and massive granular pyrite between 10 and 30 mbsf, although the fragments of massive pyrite recovered throughout this section may represent incompletely cored pyrite-anhydrite breccias. The pyrite occurs locally as discrete pyritization halos at the margins of anhydrite veins. Fragments of pyrite-silica breccia were also recovered with massive pyrite, and a single altered basalt clast was recovered at 16 mbsf.

Between 30 and 50 mbsf, recovery from Hole 957P was poor, but pyrite-silica breccias were cored in several sections. These samples are likely fragments of the same pyrite-silica breccias recovered near the top of the stockwork zone in the TAG-1 area (see Fig. 1). However, the continuity of this material and the relationship between the massive pyrite clasts and the pyrite-silica clasts could not be determined. Silicified basalt clasts occur in pyrite-silica breccias as shallow as 16.7 mbsf. Below 45 mbsf, silicified wallrock clasts and altered basalt fragments occur throughout the pyrite-silica breccias and may be part of the sub-seafloor stockwork. The basalt clasts are distinctly angular but show extensive replacement by quartz and pyrite. They increase in abundance to about 57 mbsf, where large clasts of silicified wallrock breccia were recovered among several sections of drill cuttings. Pieces of massive, granular pyrite within this lower section of core, and in drill cuttings or fill recovered from the bottom of the hole, indicate that pyrite may be an important constituent of the breccias down to at least 50 mbsf.

## Veining

Although recovery of discrete anhydrite veins was limited in comparison to core from the TAG-1 area, most of the matrix anhydrite appears to be related to veining. Anhydrite occurs as matrix material in nodular pyrite-anhydrite breccias to a depth of about 10 mbsf and mainly in vein networks in the massive brecciated pyrite between 10 and 25 mbsf. The abundance of anhydrite diminishes below about 30 mbsf and is rare in the pyrite-silica breccias below about 35 mbsf. Quartz veining is rare, except in the pyrite-silica breccias and silicified wallrock breccias, where it occurs mainly within the clasts. Pyrite veining is common in larger clasts of pyrite-silica breccia and in the silicified wallrock breccias at depth, and much of the massive, brecciated pyrite higher up in the core may be vein-related.

## Mineralization

Pyrite accounts for nearly 65 vol% (ranging from 50 to 100 vol%) of the core recovered from the upper 30 m of the mound in the TAG-5 area, and at least 50 vol% from about 30 mbsf to the maximum depth cored. Chalcopyrite is also an important constituent of the massive pyrite-anhydrite breccias (5–10 vol%), mainly in association with anhydrite veins, but also locally replacing massive granular pyrite. Two samples of pyrite-anhydrite breccia at 8 and 16 mbsf contain about 3.5 wt% Cu, and samples of pyritic drill cuttings from the base of the mound contain between 6 and 13 wt% Cu. Concentrations of Zn in these samples are low (<0.5 wt% Zn).

## Interpretation

The section of the mound cored in Holes 957O and 957P most closely resembles that of Holes 957C, 957E, 957F, and 957G in the TAG-1 area (see Fig. 1). Although the top of the stockwork could not be precisely determined from the core recovered in Hole 957P, the

presence of numerous altered basalt clasts and silicified wallrock fragments below 45 mbsf suggests that a portion of the stockwork zone occurs at the bottom of the hole. The top of the quartz stockwork in Hole 957E (see "Stratigraphy" section, Chapter 7, this volume) is at a similar depth, suggesting that the thickness of the mound beneath the northern part of the upper terrace may be similar to that in the TAG-1 area. The abundance of pyrite as cement and vein material in the lower part of the section at TAG-5 suggests that this part of the mound may be underlain by pyritic stockwork and that the sulfide-rich portion of the stockwork zone extends at least to the northern edge of the upper terrace. This style of mineralization differs somewhat from the quartz-pyrite vein network beneath the TAG-1 area and further suggests that the stockwork beneath the TAG mound may be locally heterogeneous (e.g., quartz-rich pyritic or chloritic).

The narrow zone of pyrite-anhydrite breccias (<10 m thick) near the top of the mound at TAG-5 suggests that this area may be close to the outer margin of the anhydrite-rich zone first encountered at TAG-1. Although anhydrite is much less abundant at TAG-5 than nearer the main upflow zone at TAG-1, its proximity to the top of the mound may indicate that this has been an area of recent high-temperature upflow in the TAG-5 area. Replacement of pyrite by chalcopyrite in the pyrite-anhydrite breccias also implies a phase of thermally intensifying hydrothermal activity. The fact that most of the sulfide-rich material recovered in the TAG-5 area consists of massive brecciated pyrite and vein-related pyrite rather than clastic sulfide debris, as in other areas of the mound, is consistent with precipitation during a period of high-temperature upflow.

## SULFIDE PETROLOGY AND GEOCHEMISTRY

### Introduction

Two holes were drilled in the northern part of the TAG mound (TAG-5 area; see Fig. 3, Chapter 1, this volume). Hole 957P is located 35–40 m north of the TAG-1 area and 20 m north-northeast of the central Black Smoker Complex; it was cored to a depth of 59.4 mbsf with recovery of 7.7%. Hole 957O is located 10–15 m east-northeast of Hole 957P and was cored to a depth of 20.5 mbsf with recovery of 6.2%. Rock types encountered in Holes 957O and 957P include massive granular pyrite (Type 5), pyrite breccia (Type 6), pyrite-anhydrite breccia (Type 7), pyrite-silica breccia (Type 9), and silicified wallrock breccia (Type 10). A list of the visual core descriptions is given in Table 2 (back pocket), and graphical summary logs are illustrated in Figures 2A and 2B. The very low recovery (not counting drill cuttings ~3.5%) throughout much of the section at Hole 957P makes the stratigraphy difficult to assess.

Nodular pyrite and pyrite-anhydrite breccias are the dominant rock types in Hole 957O (Cores 158-957O-2R and 3R). A single pebble-sized piece of porous massive pyrite (curated as Sample 158-957O-2R-1, Piece 1), was actually recovered from Core 158-957O-1R. Below 15.9 mbsf in Core 158-957O-4R, the nodular pyrite and nodular pyrite-anhydrite breccias grade into pyrite-anhydrite breccias with anhydrite veining and into vein-related massive granular pyrite. Pyrite-silica breccias also occur in this interval (15.9–20.5 mbsf). The sequence of rock types recovered from Hole 957P is similar to that described above. Pyrite-anhydrite breccias (locally nodular) were recovered in Cores 158-957P-1R, 2R, and 6R, to a depth of 30.1 mbsf. Massive granular pyrite (commonly vein related) is relatively abundant throughout the section, with two or three pieces of massive granular pyrite making up the entire recovery from Cores 158-957P-3R, 4R, and 5R. Pyrite-silica breccias underlie the pyrite-anhydrite breccias and dominate the recovered material below 30.1 mbsf (Cores 158-957P-7R to 12R). Pieces of silicified wallrock breccia (with clasts exhibiting basaltic textures) were recovered in Sections 158-957P-8R, 11R, and 12R (i.e., below 35.1 mbsf). The final core from Hole 957P (Sections 158-957P-12R-1 to 12R-4) contained 2.1 m of drill cuttings, in the form of pyrite-anhydrite-quartz sand and gravel, with pieces of gray and black chert (maximum 8 mm in size). A subsequent wash core of similar material (Core 158-957P-13W) was also collected from the interval between 16 and 59 mbsf.

#### *Massive Pyrite (Type 5)*

One piece of porous massive pyrite (Type 5a) was recovered from the depth interval 0–7.9 mbsf (curated as Sample 158-957O-2R-1, Piece 1), and is distinctly fine-grained, porous, and chalcopyrite rich (10 vol%). A second small piece of porous massive pyrite, which displays colloform textures, was recovered between 35.1 and 40.1 mbsf. This latter sample is unlike any other material recovered in this hole, as it contains minor quantities of discrete pyrrhotite grains. In thin section, a porous network of euhedral pyrite is overgrown by chalcopyrite and minor sphalerite (Fig. 3). Pyrrhotite occurs as overgrowth and as euhedral grains between these aggregates. Late amorphous silica lines voids, and a trace of marcasite is disseminated along fractures.

Massive granular pyrite (Type 5c) occurs in samples from between 15.9 mbsf and the bottom of Hole 957O, and between 11.9 mbsf and the bottom of Hole 957P. Two associations have been recognized, one with anhydrite veining and pyrite-anhydrite breccias, and the other with pyrite-silica breccias. The anhydrite-related massive granular pyrite occurs in samples from 15.9 mbsf to the bottom of Hole 957O and from 11.9 to 30.1 mbsf in Hole 957P. Pyrite is present as granular or crustiform-banded aggregates and intergrown with chalcopyrite (up to 10 vol%). Anhydrite comprises up to 30 vol% (where samples are transitional to vein-related pyrite-anhydrite breccias), as a matrix to the disseminated sulfide, in vugs, and in veins. Silica is rare. Small samples of granular pyrite, with only a trace of chalcopyrite (e.g., Sample 158-957P-2R-1, Piece 2) are identical in texture to clasts seen within pyrite- and pyrite-anhydrite breccias (Fig. 4) and are likely derived from the incomplete recovery of such breccias.

Massive granular pyrite samples associated with pyrite-silica breccias recovered from below 31.1 mbsf in Hole 957P are coarse grained and contain significant silica. Some samples exhibit clastic textures in the form of nodular pyrite regions in a massive pyrite aggregate (e.g., Sample 158-957P-8R-1, Piece 1). Most samples of massive granular pyrite are transitional in composition and texture between massive granular pyrite and pyrite-silica breccias (Fig. 5). Massive pyrite is commonly seen to include remnant patches of chert, dark gray silica, and silicified altered basalt material (e.g., Samples 158-957P-10R-1, Piece 2, and 12R-4, Piece 11). The presence of red chert, pyrite-silica breccia, and altered basalt within massive granular pyrite pieces suggests that the rock could have formed by pyritization of an existing pyrite-silica or silicified wallrock breccia. Locally, the massive granular pyrite is also transitional to more porous pyrite-chalcopyrite intergrowths, which appear to be vein related (see discussion of veining in "Hydrothermal Alteration" section, this chapter).

#### *Pyrite Breccias (Type 6)*

Nodular pyrite breccia (Type 6a) occurs in the core from the upper parts of Hole 957O (7.9–10.9 mbsf); it is composed of nodular pyrite clasts and angular aggregates (1 cm diameter), in a matrix of fine sandy pyrite and anhydrite (maximum 20 vol% anhydrite) (Fig. 6). Silica (maximum 20 vol%) is present in the matrix (particularly in Sample 158-957O-2R-1, Piece 7). These samples differ from other breccias from Holes 957O and 957P in the presence of silica, and lower proportions of anhydrite in the matrix.

#### *Pyrite-Anhydrite Breccias (Type 7)*

Massive pyrite-anhydrite breccias (Type 7a; Fig. 7) and nodular pyrite-anhydrite breccias (Type 7b; Fig. 8) occur in cores from Hole

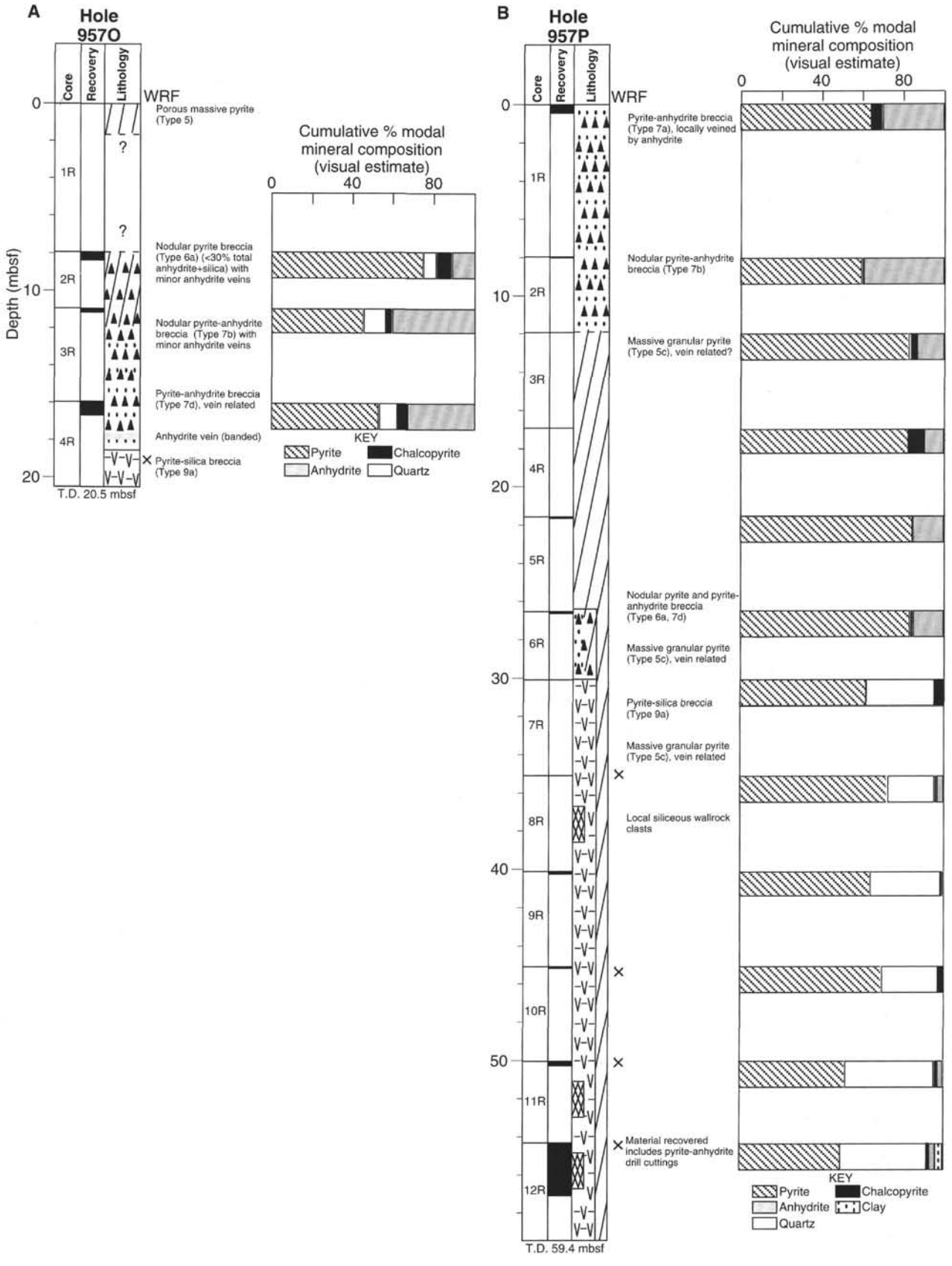


Figure 2. Schematic stratigraphic sections for Holes 957O (**A**) and 957P (**B**). Wallrock fragments (WRF) are shown by a small ×. TD = total depth. Note that a single small piece in Core 158-957O-1R-1 was curated as Core 158-957O-2R-1 (Piece 1).

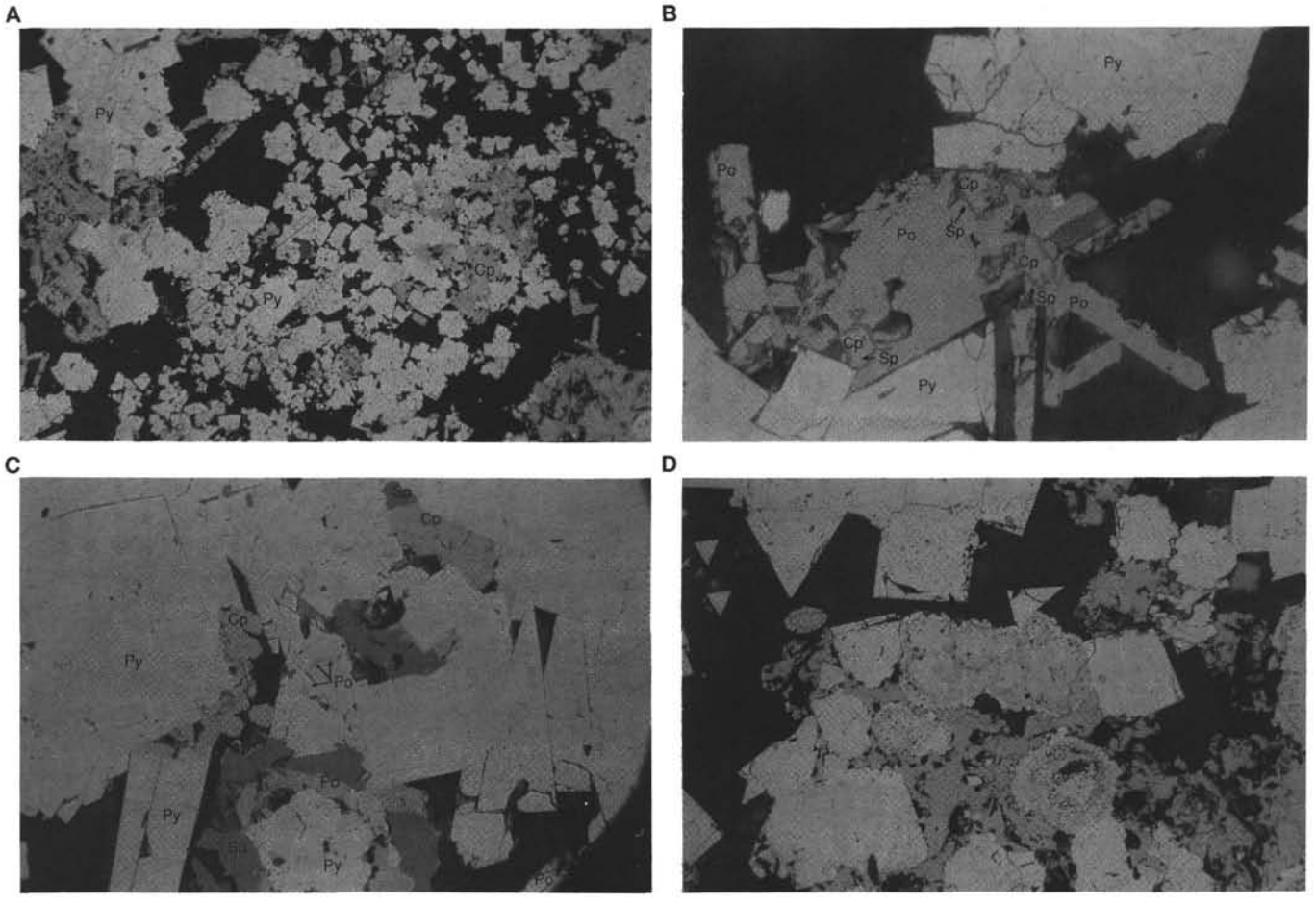


Figure 3. Thin section photomicrographs of porous massive pyrite (Type 5a) unusually enriched in pyrrhotite (Sample 158-957P-8R-1, Piece 7, 27–31 cm). **A.** General view of the mineralogical assemblage. Chalcopyrite (medium gray; Cp) is interstitial between the euhedral pyrite grains and aggregates (light gray; Py). Porosity (black) is high, and the open spaces contain local, large-bladed pyrrhotite crystals (Po). Reflected light, field of view = 1.5 mm. **B.** Detail of large pyrrhotite blades (medium gray, Po) interstitial between euhedral pyrite crystals (light gray; Py). Note the straight contact between pyrrhotite and pyrite crystals. A sphalerite rim (Sp) occurs at the contact between chalcopyrite (Cp) and pyrrhotite. Reflected light, field of view = 300 µm. **C.** Pyrite (light gray; Py), pyrrhotite (medium gray, Po), chalcopyrite (medium gray; Cp), sphalerite (dark gray; Sp) assemblage. Pyrrhotite occurs as interstitial laths and as small inclusions (arrows) in the pyrite grain at the center of the photo. Reflected light, field of view = 300 µm. **D.** Spheroidal pyrite (light gray with many inclusions) overgrown by euhedral pyrite (light gray). Chalcopyrite (medium gray) is interstitial. Reflected light, field of view = 750 µm.

957O from 10.9 to 20.5 mbsf; they were also recovered from shallow to intermediate depths in Hole 957P (0.0–30.1 mbsf). The breccias from Hole 957O (Fig. 9) are more nodular than those from Hole 957P; otherwise, they are similar in texture and mineralogy. They contain nodular to angular clasts of pyrite (as large as 2 cm in diameter) and aggregates of chalcopyrite (smaller than 3 mm diameter). In thin section, the chalcopyrite is seen to overgrow and infill porous pyrite aggregates (Fig. 10). The breccias are matrix-supported by fine- to medium-grained pyrite and anhydrite. Anhydrite occurs in vugs, as irregular veins, and as matrix; it comprises up to 60 vol% of the rock. The layer of anhydrite on the outer surface of Sample 158-957O-2R-1 (Piece 2) contains minor, very fine-grained, hexagonal pyrrhotite, intergrown with and as late overgrowths on, coarse anhydrite. In Section 158-957P-1R-1, some of the pyrite-anhydrite breccia pieces contain large (3 cm diameter) clasts of very fine-grained pyrite and chalcopyrite (Samples 158-957P-1R-1, Pieces 1, 2, and 9). Similar breccias were recovered from Hole 957H (see "Sulfide Petrology and Geochemistry" section, Chapter 8, this volume).

The proportion of anhydrite and vein-related mineralization increase in samples recovered below about 10 mbsf in Holes 957O and 957P. Vein-related pyrite-anhydrite breccia (Type 7d) was recovered in Hole 957O (Section 158-957O-4R-1, Pieces 1–4, 11–14, and 19), and a few pieces were also sampled in Hole 957P (Sections 158-957P-1R-1, Piece 9, and 6R-1, Piece 2). These samples are characterized by fine- to coarse-grained pyrite and chalcopyrite disseminated in anhydrite, with a banded texture (Fig. 11). This sample is pink as a result of inclusions of very fine-grained Fe-oxide or oxyhydroxide in anhydrite in the matrix (Sample 158-957P-1R-1, Piece 10). Anhydrite is generally equal or greater in abundance to the sulfides, and this type of breccia is transitional to anhydrite veins (Type 11), one small piece of which was recovered (Sample 158-957O-4R-1, Piece 2).

### *Pyrite-Silica Breccia (Type 9a)*

Pyrite-silica breccias recovered from Hole 957O below 15.9 mbsf, and from Hole 957P below 30.1 mbsf, exhibit similar textures and mineral compositions. Samples from deeper in Hole 957P (below 35.1 mbsf) record a more complex history of brecciation, veining, and alteration. Nodular pyrite-silica breccias consist of small (<1 cm), rounded pyrite aggregates in a matrix of pale gray silica (Fig. 12). A second, more complex type of pyrite-silica breccia is more abundant and is transitional between massive granular pyrite and silicified wallrock breccia, depending on the relative proportions of py-

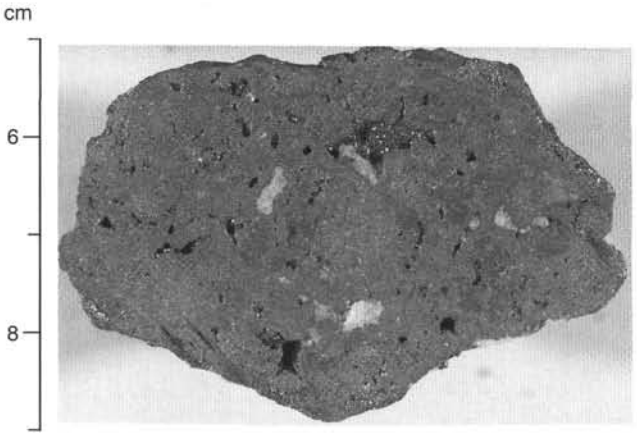


Figure 4. Massive granular pyrite (Type 5c) composed of fine-grained euhedral pyrite. Anhydrite (white) is a late mineral filling vugs. Chalcopyrite is a minor mineral disseminated in pyrite. Sample 158-957P-3R-1 (Piece 2, 5–9 cm).

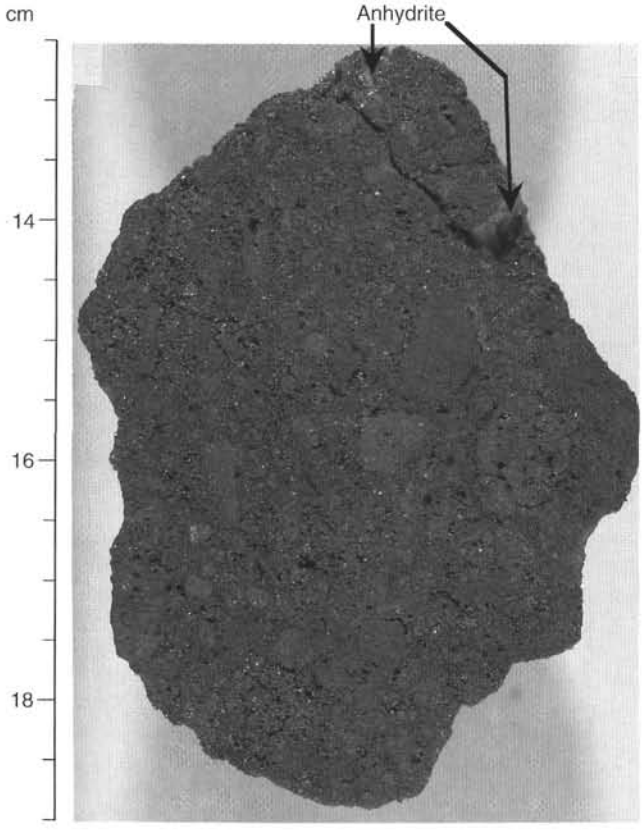


Figure 6. Nodular pyrite breccia (Type 6a). Rounded to angular, fine-grained pyrite clasts in a pyrite matrix. Anhydrite (light gray, labeled) occurs disseminated in the matrix and as small veins. Minor silica is present in the matrix. Chalcopyrite occurs as millimeter-sized clasts and disseminations in the matrix. Sample 158-957O-2R-1 (Piece 4, 13–19 cm).

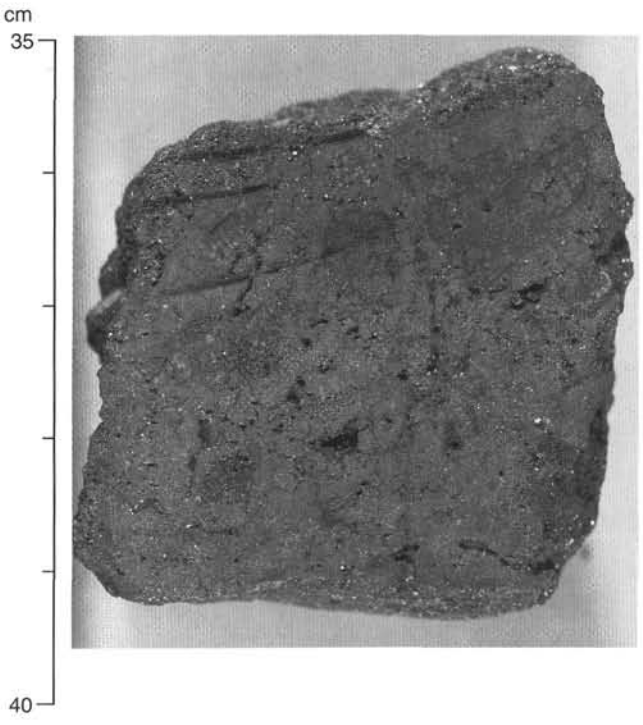


Figure 5. Massive granular pyrite (Type 5c) composed of fine-grained euhedral pyrite. Note the large angular clast of pyrite-silica breccia (dark gray, top right of piece) with disseminated sulfides and sulfide aggregates on the upper right part of the sample. Sample 158-957P-11R-1 (Piece 8, 35–40 cm).

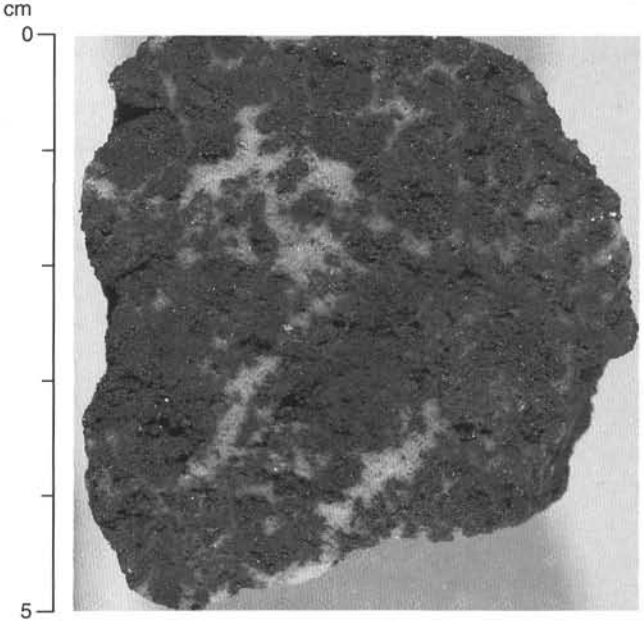


Figure 7. Pyrite-anhydrite breccia (Type 7a). Medium-grained euhedral crystals of anhydrite (white) occur as a matrix around massive fine-grained pyrite aggregates and clasts. Chalcopyrite is locally enriched in the clasts. Sample 158-957P-1R-1 (Piece 1, 0–5 cm).

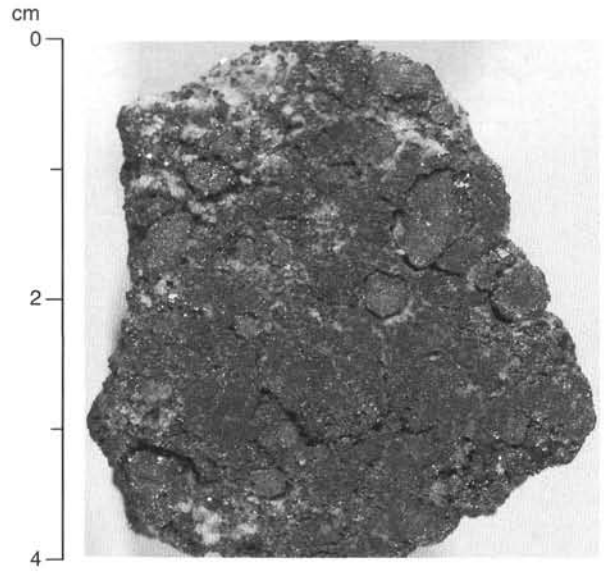


Figure 8. Nodular pyrite-anhydrite breccia (Type 7b). Pyrite occurs as centimeter-sized aggregates and rounded clasts and is disseminated with anhydrite in the matrix. The sample is composed of 30 vol% anhydrite (visual estimate). Sample 158-957P-2R-1 (Piece 1, 0–4 cm).

rite or altered basalt (Fig. 13). The breccia consists of coarse, poorly sorted pyrite aggregates (maximum 1.5 cm diameter), in a matrix of fine- to very fine-grained dark gray silica with coarse, disseminated pyrite. Anhydrite is common and is confined to vugs and late veining (preserved as coatings on some pieces). These breccias contain clasts of an earlier generation of pale gray, fine-grained pyrite-silica breccia (Fig. 14), indicating that at least two stages of brecciation have occurred.

Clasts of silicified and pyritized basalt occur in the pyrite-silica breccias between 15.9 mbsf and the base of Hole 957O (Sample 158-957O-4R-1, Piece 18). In core from Hole 957P, altered basalt clasts were observed only in the breccias recovered from below 35.1 mbsf. Many altered basalt clasts are cut by networks of 0.5 mm pyrite-quartz veinlets, and some are rimmed by pyrite. Where the altered basalt material is most abundant, pieces are transitional in texture and mineralogy to silicified wallrock breccia. The altered basalt clasts are described in detail in the "Hydrothermal Alteration" section (this chapter).

### *Silicified Wallrock Breccia (Type 10a)*

A few small pieces of silicified wallrock breccia occur in core from Hole 957P. They are composed of clasts of altered basalt in a pyrite-silica matrix. The altered basalt occurs as clasts with a gray to buff, quartz-pyrite-chlorite(?) assemblage, with pyrite aggregates of 1 mm diameter (Fig. 15). In the core from below 45.1 mbsf in Hole 957P, the altered basalt is intensely pyritized and enclosed in massive granular pyrite, possibly of vein-related origin. A more detailed description of the altered basalt and related veining and brecciation is in the "Hydrothermal Alteration" section (this chapter).

### *Pyrite-Anhydrite-Quartz Drill Cuttings*

The last two cores recovered from Hole 957P contain abundant sand-sized drill cuttings. The 2.14 m of this material recovered in Core 158-957P-12R (from a depth interval of 54.4–59.4 mbsf) is comprised of abundant, very fine- to fine-grained pyrite; minor amounts of fine-grained quartz and anhydrite; and minor amounts of Fe-oxide. Material in the core grades from fine to coarser with depth.

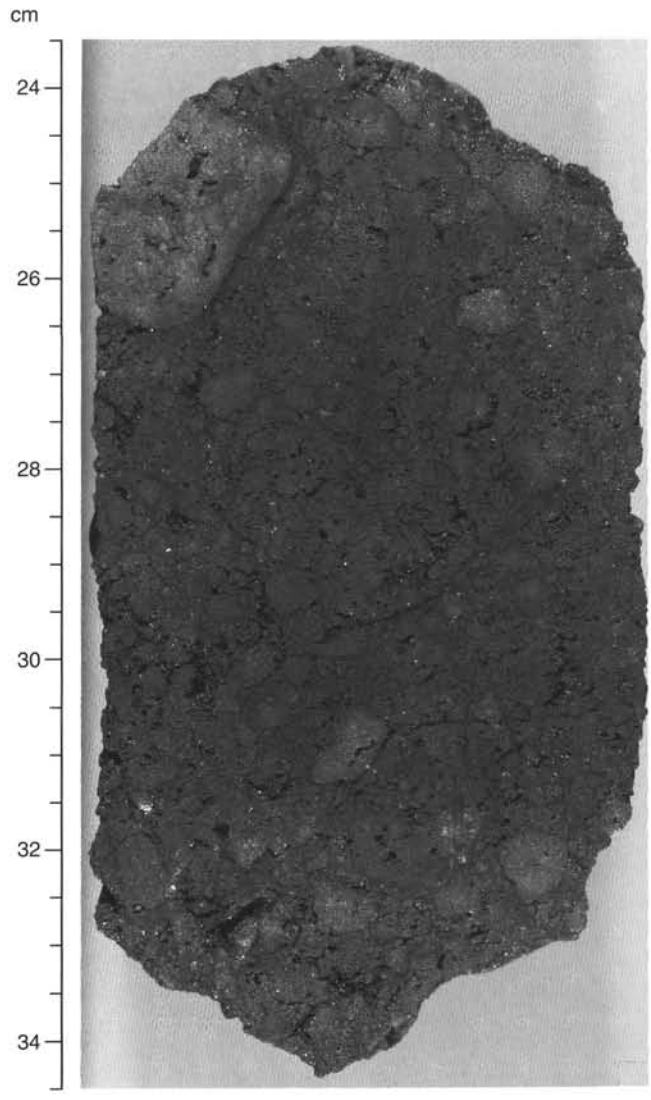


Figure 9. Nodular pyrite-anhydrite breccia (Type 7b). This sample is a clast-supported breccia in which the clasts are mainly pyrite. Some clasts are composed of coarse, granular pyrite similar in texture to samples recovered elsewhere in the core (cf. Fig. 4). Sample 158-957O-4R-1 (Piece 6, 23–35 cm).

This sorting may be related to settling in the core during drilling and recovery. Cobbles of massive granular pyrite, pyrite-silica breccia, and silicified wallrock breccia were embedded in the sand 107–140 cm from the top of Section 158-957P-12R-1, 0–55 cm from the top of Section 158-957P-12R-3, and 0–29 and 64–70 m from the top of Section 158-957P-12R-4. Core 158-957P-13W is a wash core recovered from 15 to 54 mbsf; it is comprised of 2.5 m of pyrite-anhydrite sand and gravel with dark gray to black chert clasts up to 8 mm in size. Section 158-957P-13W-1 is finer grained than Section 158-957P-13W-2. It is unclear whether this material in Cores 158-957P-12R and 13W represents matrix material that surrounds the clasts and cobbles recovered in cores from Hole 957P, or if they are drill cuttings.

## Sulfide Geochemistry

Four samples of core material from Holes 957O and 957P in the TAG-5 area northeast of the Black Smoker Complex were analyzed by AAS and CHNS. The results are summarized in Table 3. The two

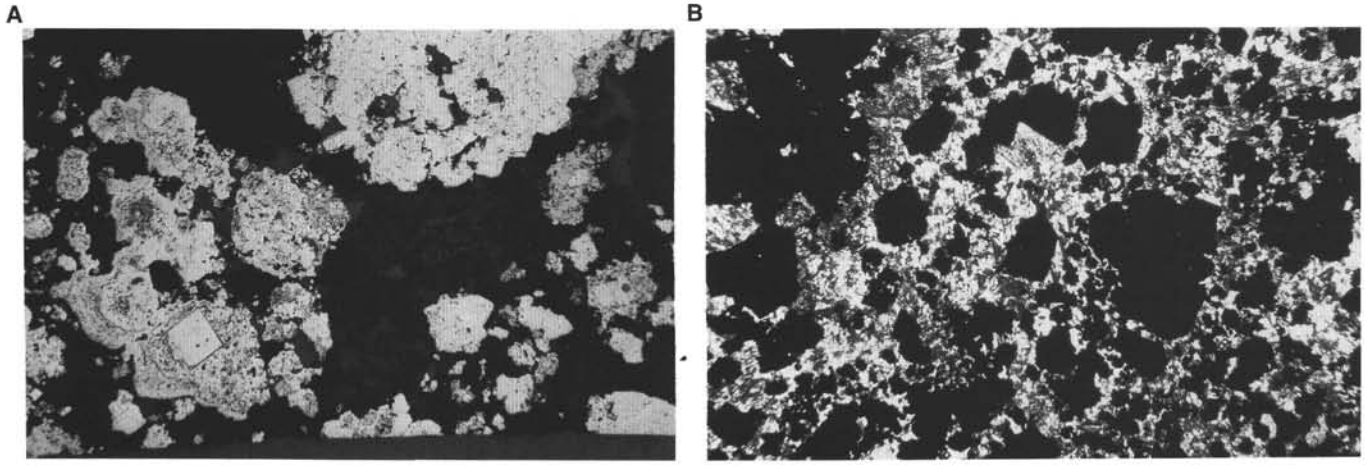


Figure 10. Thin-section photomicrographs of pyrite-anhydrite breccia in Sample 158-957O-2R-1 (Piece 5, thin section from 22–24 cm), Type 7a. **A.** Pyrite and marcasite growth layers (white and light gray) in a matrix of anhydrite crystals (dark gray). Note the large euhedral pyrite crystal at the center of the pyrite + marcasite assemblage. Reflected light, field of view = 300 µm. **B.** Pyrite and chalcopyrite aggregates (black) in anhydrite matrix. Transmitted light, field of view = 6 mm.

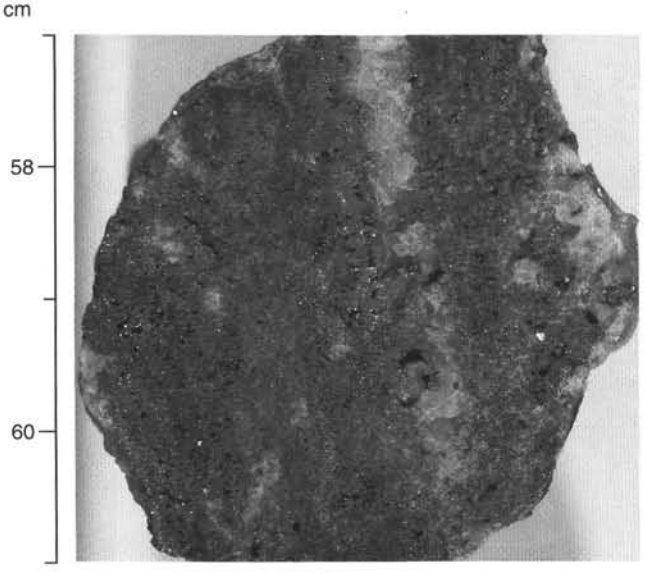


Figure 11. Vein-related pyrite-anhydrite breccia (Type 7d). Anhydrite (white) with disseminated, fine-grained pyrite and chalcopyrite forming massive and crustiform, banded aggregates. Coarse, granular anhydrite lines vugs and forms a 4-mm-wide vein. Sample 158-957O-4R-1 (Piece 12, 57–61 cm).

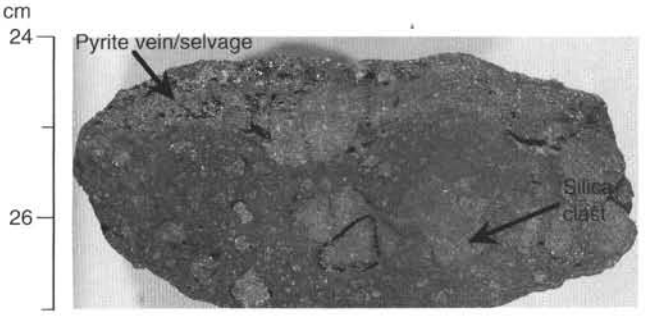


Figure 12. Pyrite-silica breccia (Type 9a). Most of the clasts are massive pyrite. Pyrite occurs also as disseminated grains in the pale gray silica matrix and is locally enriched around a silica clast (arrow). A pyrite vein (labeled) is associated with anhydrite. Sample 158-957P-10R-1 (Piece 6, 24–27 cm).

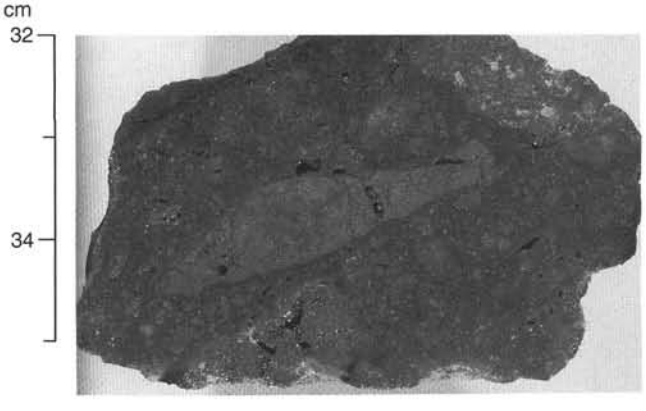


Figure 13. Pyrite-silica breccia (Type 9a) with silicified basalt clasts. Two large, angular, silicified basalt clasts are enclosed in a matrix of dark gray silica with disseminated pyrite. The clast on the edge of the piece contains aggregates of tan clay. Both clasts are cut by a network of thin pyrite-quartz veins, and the grain in the center is fractured and cut by a later pyrite vein. The smaller clasts are massive granular pyrite. Sample 158-957P-12R-2 (Piece 7, 32–35 cm).

samples from Hole 957O consist of nodular pyrite breccia (Sample 158-957O-2R-1, Piece 5) from 8.1 mbsf and pyrite-anhydrite breccia (Sample 158-957O-4R-1, Piece 9) from 16.4 mbsf. The two samples of drill cuttings from Hole 957P that have been analyzed consist of pyrite (sand- and silt-sized) and pyrite-anhydrite (sand- and gravel-sized), respectively. The high Cu contents (3.10%–13.30) of the TAG-5 samples are similar to, or exceed, those of the rocks of the TAG-1 area from the surface down to about 40 mbsf. Lead could not be analyzed because of the failure of the hollow cathode lamp.

### *Composition of Rock Types Analyzed in the TAG-5 Area*

*Nodular Pyrite Breccia (Type 6a)*

Sample 158-957O-2R-1, Piece 5, had S and Fe concentrations of 45.1 and 33.0 wt%, respectively. The Cu content was high (3.7 wt%),

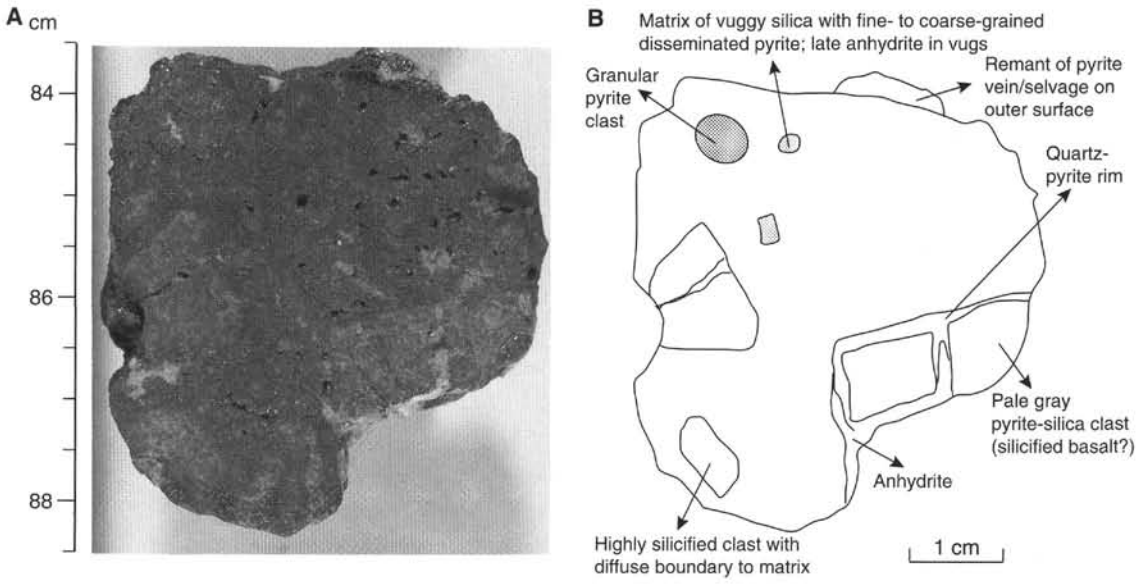


Figure 14. Pyrite-silica breccia (Type 9a). **A.** Porous, dark gray silica matrix with coarse, disseminated pyrite and several granular pyrite aggregates. Rounded to subangular silica clasts (pale gray) contain fine disseminated pyrite; these clasts may be highly altered and silicified basalt. White anhydrite fills vugs and fractures as well as coats part of the outside of the sample. **B.** Sketch showing the distribution of different clast types. Sample 158-957O-4R-1 (Piece 18, 83.5–89.5 cm).

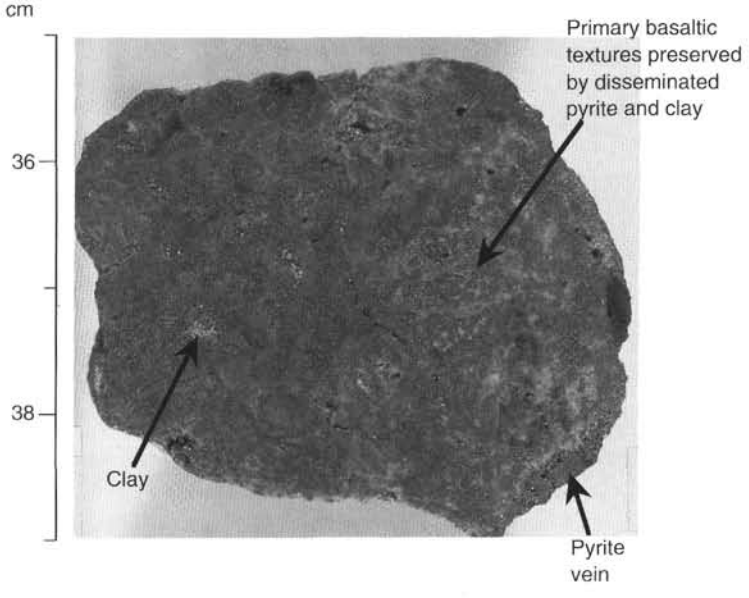


Figure 15. Silicified wallrock breccia (Type 10a). A clast of silicified basalt is bounded by a massive pyrite vein (labeled). Most of the sample is quartz with disseminated pyrite. In some places, primary basaltic textures are preserved by disseminated pyrite and clay in the silica matrix. Other parts of the sample have diffuse patches in which the textures are obscured by more intensive silicification and pyritization. Sample 158-957P-12R-4 (Piece 2, 34–39 cm).

**Table 3. AAS and CHNS analyses of sulfide samples from Holes 957O and 957P.**

| Core, section, interval (cm) | Size fraction or piece no. | Depth (mbsf) | Type | Rock type | S (wt%) | Fe (wt%) | Zn (wt%) | Cu (wt%) | Ag (ppm) | Cd (ppm) |
|---|---|---|---|---|---|---|---|---|---|---|
| 158-957O- | | | | | | | | | | |
| 2R-1, 22–24 | 5 | 8.1 | 6a | Nodular pyrite breccia | 45.1 | 33.0 | 0.03 | 3.71 | 4.5 | ND |
| 4R-1, 45–50 | 9 | 16.35 | 7a | Pyrite-anhydrite breccia | 51.4 | 42.7 | 0.04 | 3.10 | 4.3 | ND |
| 158-957P- | | | | | | | | | | |
| 12R-1, 15–100 | >420 µm | 54.4 | — | Drill cuttings, pyrite sand and silt | 37.8 | 34.4 | 0.28 | 8.22 | 11.1 | 7.4 |
| 12R-1, 15–100 | 420–63 µm | 54.4 | — | Drill cuttings, pyrite sand and silt | 40.6 | 36.4 | 0.33 | 10.20 | 11.7 | 9.0 |
| 12R-1, 15–100 | <63 µm | 54.4 | — | Drill cuttings, pyrite sand and silt | 41.6 | 36.9 | 0.53 | 13.30 | 13.1 | 13.5 |
| 13W-1+2, 70–100 | — | — | — | Drill cuttings, pyrite-anhydrite sand and gravel | 46.1 | 39.6 | 0.15 | 6.66 | 8.3 | 2.9 |

Notes: ND = not determined. Pb not analyzed.

and concentrations of trace elements were low. The sample contained 0.03 wt% Zn and 4.5 ppm Ag, but concentrations of Cd were below the detection limit. Metal concentrations of Sample 158-957O-29-1, Piece 5, are within the range of similar nodular pyrite breccia samples taken from the TAG-1 and TAG-2 areas (e.g., Samples 158-957F-1N-1, Piece 8, and 158-957H-1N-1, Piece 13).

*Pyrite-Anhydrite Breccia (Type 7a)*

Sample 158-957O-4R-1, Piece 9, was rich in S and Fe (51.4 and 42.7 wt%, respectively) and may have preferentially been a pyrite clast in these extremely heterogeneous rocks. The Cu content was high (3.1 wt%), and concentrations of Zn, Ag, and Cd low (0.04 wt%, 4.3 ppm, and <0.1 ppm, respectively), similar to the nodular pyrite breccia.

*Pyrite and Pyrite-Anhydrite Drill Cuttings*

Sand- and silt-sized pyritic material from Core 158-957P-12R-1 was combined into one sample from the interval 15–100 cm and sifted into three grain-size fractions: >420 µm, 420–63 µm, and <63 µm. All grain sizes had high concentrations of Cu (i.e., ranging from 8.2 to 13.3 wt%), similar to the Fe-oxides and sulfide sand from the TAG-2 area. Copper appeared to be preferentially associated with the fine fractions, suggesting that the chalcopyrite is more easily ground by the drilling operations than the pyrite. The content of S increased from 37.8 wt% in the coarse fraction to 41.6 wt% in the fine fraction, whereas Fe increased from 34.4 to 36.9 wt%. Concentrations of Zn, Ag, and Cd were low (Zn between 0.15 and 0.53 wt% [8.3–13.1 ppm]; Ag and Cd from 2.9 to 13.5 ppm). Nevertheless, like Cu they showed a trend of increasing concentrations with decreasing grain size.

Sand- and gravel-sized pyrite-anhydrite material from the interval between 50 and 58 cm from Sections 158-957P-13W-1 and 13W-2 was combined into a single sample for future use as an interlaboratory sulfide standard. The chemical composition was similar to that of the pyrite sand and silt, especially with regard to the high Cu concentration (6.7 wt%). However, concentrations of S and Fe were higher (46.1 and 39.6 wt%) and concentrations of Zn, Ag, and Cd lower (0.15 wt%, 8.3 ppm, and 2.9 ppm, respectively).

## Summary

Hole 957P is located approximately the same distance from the Black Smoker Complex as the TAG-1 area (~20 m), and Hole 957O is located ~30–35 m from the Black Smoker Complex (i.e., 10–15 m east-northeast of Hole 957P). Rock types recovered from the upper 7.9 m of Holes 957O and 957P include porous massive pyrite and pyrite-anhydrite breccias with incorporated surface material and narrow, irregular veins of anhydrite. Material recovered from shallow depths in Hole 957O differs from material from Hole 957P in containing greater amounts of silica. In the core from Holes 957O (between 10.9 and 18 mbsf) and 957P (7.9 and 31.1 mbsf), nodular pyrite-anhydrite breccias and vein-related massive granular pyrite and pyrite-anhydrite breccias dominate. Anhydrite abundances in core from these depth intervals and shallower are generally high (7–60 vol% by visual estimate). Between depths of 11.9 and 26.5 mbsf in Hole 957P, the only material recovered was vein-related massive granular pyrite with up to 20 vol% anhydrite. This vein-related material is classified as Stage 5 veining using the criteria described in the "Sulfide Petrology and Geochemistry" section (Chapter 7, this volume). The low recovery over this depth interval (1%–2%) makes it difficult to interpret whether this zone also contains thick veins of massive anhydrite similar to those recovered in core from Hole 957C in the TAG-1 area, wide zones of pyrite-rich vein material, pyrite-anhydrite breccias similar to those recovered from shallower depths in Hole 957P, or some other rock type. In core recovered from below 31.1 mbsf in Hole 957P, and at depths between 15.9 and 20.5 mbsf in Hole 957O, pyrite-silica breccias and vein-related massive granular pyrite dominate. The pyrite-silica breccias contain only trace amounts of anhydrite, as grains on the outer surfaces of samples. Anhydrite is present in greater amounts (up to 30 vol% by visual estimate) in the vein-related massive granular pyrite samples. Clasts of silicified wallrock occur in core recovered from below depths of 15.9 and 35.1 mbsf in Holes 957O and 957P, respectively, corresponding to the transition from pyrite-anhydrite to pyrite-silica breccias. Textures of the pyrite-silica breccias record multiple stages of brecciation and veining. Pyritization is common in breccias recovered from below 45.1 mbsf in Hole 957P.

A difference in the core recovered from the TAG-5 area compared with that from other areas is the presence of very fine grains (500 µm; visible in hand specimen) of euhedral hexagonal pyrrhotite. It occurs intergrown with anhydrite in a late anhydrite vein that coats the surface of a nodular pyrite breccia piece (Sample 158-957O-2R-1, Piece 2) that was recovered from a depth less than 10.9 mbsf in Hole 957O. It also occurs as a late phase overgrowing pyrite and filling interstices in a piece of porous massive pyrite (Sample 158-957P-8R-1, Piece 7) that was recovered from a depth interval of 35.1 to 40.1 mbsf in Hole 957P. The only other reported occurrences of pyrrhotite in samples from the active TAG mound are as rare 5–10 µm anhedral inclusions in pyrite in two samples recovered from Hole 957E in the TAG-1 area (Samples 158-957E-11R-1, Piece 9, and 18R-1, Piece 5), and as 20–30 µm euhedral grains in a sulfide crust sample recovered from the surface of the Black Smoker Complex (Tivey et al., 1995). In all of these cases, including the TAG-5 samples, pyrrhotite is present in only trace to minor amounts.

The general trend, with depth observed in core recovered from Holes 957O and 957P, from nodular pyrite to pyrite-anhydrite to pyrite-silica breccias, with a shallow anhydrite-rich zone overlying a more siliceous zone that includes clasts of silicified wallrock, is similar to trends observed in Holes 957C and 957E of the TAG-1 area, and in Hole 957H of the TAG-2 area. The trend of observed veining types with depth at TAG-5, from dominantly anhydrite-pyrite-chalcopyrite veining dominating at shallow depths, and quartz-pyrite veining being more common at greater depths, is also similar to veining trends observed in cores recovered from the TAG-1 and TAG-2 areas.

## HYDROTHERMAL ALTERATION

Altered basaltic material was recovered from two holes (Holes 957O and 957P) from the TAG-5 area on the northern side of the TAG mound (see Fig. 2). Because of time constraints at the end of the leg, no thin sections were made of altered basaltic material from these cores and all descriptions are based solely on hand specimen observations. Clasts of silicified basalt occur in pyrite-silica breccias from both holes, in core recovered from 15.9 to 20.5 mbsf in Hole 957O and from 35.1 mbsf to the bottom of the hole at 59.4 mbsf in Hole 957P. Silicified and pyritized basalt clasts also occur within samples of massive pyrite recovered from the lowermost part of Hole 957P (45.1–59.4 mbsf).

In Hole 957O, silicified basalt clasts were recovered in only one piece (Sample 158-957O-4R-1, Piece 18), at 16.74 mbsf. Gray, 1-mm to 2-cm angular clasts of basalt, replaced by quartz, chlorite, and pyrite, occur in the pyrite-silica breccia matrix of dark gray, fine-grained quartz and 0.1- to 3-mm grains and aggregates of pyrite. Some clasts are cut by a network of fine (0.1–0.5 mm) quartz + pyrite veinlets. Clasts are also commonly partly rimmed by a 0.5-mm layer of pyrite, and late anhydrite occurs filling pores and in 1-mm veins.

In Hole 957P, 1-mm to 5-cm, round to angular to irregularly shaped, silicified basalt clasts occur in pyrite-silica breccias recovered from 35 mbsf to the bottom of the hole at 59.4 mbsf (Cores 158-957P-8R through 12R). The clasts are gray to buff and occur in a ma-

**Table 4. Index properties of samples recovered from Holes 957O and 957P.**

| Core, section, interval (cm) | Depth (mbsf) | Bulk water content (%) | Bulk density [B] (g/cm$^3$) | Bulk density [C] (g/cm$^3$) | Grain density [B] (g/cm$^3$) | Grain density [C] (g/cm$^3$) | Porosity [B] (%) | Porosity [C] (%) | Rock type (F = fragment, M = minicore) |
|---|---|---|---|---|---|---|---|---|---|
| 158-957O- | | | | | | | | | |
| 2R-1, 34–36 | 8.24 | 2.66 | 4.05 | 3.94 | 4.41 | 4.27 | 10.52 | 10.22 | Nodular pyrite breccia (M) |
| 4R-1, 29–31 | 16.19 | 1.92 | 4.27 | 4.19 | 4.55 | 4.46 | 8.00 | 7.84 | Nodular pyrite-anhydrite breccia (M) |
| 158-957P- | | | | | | | | | |
| 1R-1, 38–40 | 0.38 | 2.70 | 3.68 | 3.55 | 3.97 | 3.82 | 9.72 | 9.38 | Pyrite-anhydrite breccia (F) |
| 2R-1, 6–8 | 7.96 | 1.38 | 4.80 | 4.69 | 5.06 | 4.94 | 6.47 | 6.34 | Massive granular pyrite (F) |
| 4R-1, 1–3 | 16.91 | 0.85 | 4.80 | 4.63 | 4.96 | 4.77 | 3.98 | 3.84 | Massive granular pyrite (F) |
| 7R-1, 5–7 | 30.15 | 2.31 | 4.79 | 4.46 | 5.25 | 4.85 | 10.81 | 10.08 | Massive granular pyrite (F) |
| 8R-1, 9–11 | 35.19 | 2.81 | 4.40 | 4.09 | 4.86 | 4.48 | 12.07 | 11.23 | Porous massive pyrite (F) |
| 9R-1, 22–24 | 40.32 | 1.32 | 4.61 | 4.43 | 4.84 | 4.63 | 5.93 | 5.70 | Massive granular pyrite (F) |
| 10R-1, 10–12 | 45.20 | 1.47 | 4.41 | 4.24 | 4.64 | 4.44 | 6.32 | 6.07 | Massive granular pyrite (F) |
| 11R-1, 18–20 | 50.28 | 1.20 | 3.47 | 3.37 | 3.57 | 3.47 | 4.05 | 3.93 | Pyrite-silica breccia (F) |
| 12R-3, 67–69 | 57.03 | 1.13 | 4.19 | 5.19 | 4.35 | 5.44 | 4.63 | 5.72 | Massive granular pyrite (F) |

Note: [B] and [C] refer to the method used to calculate bulk and grain density (see "Index Properties" section, "Explanatory Notes" chapter, this volume).

trix of white to dark gray quartz + pyrite (Figs. 13, 14). The clasts are replaced by quartz, gray chlorite(?), and 0.1- to 1-mm pyrite grains and aggregates. The clasts commonly have 0.5- to 3-mm rims of pyrite, which also replaces the margins of the basaltic fragments. Many of the clasts are intensively pyritized. Concentric bands of quartz, pyrite, and a white clay mineral may indicate the presence of millimeter-sized clasts of altered basaltic glass in one sample (Sample 158-957P-12R-4, Piece 2). Silicified basalt clasts are also common in massive pyrite matrix at depths greater than 45 mbsf in Hole 957P (Cores 158-957P-10R and 12R). These basalt clasts are more intensively replaced by pyrite than those in the pyrite-silica breccias.

The breccias and massive pyrite containing silicified basalt clasts from Hole 957P have numerous veins, indicating multiple stages of veining, brecciation, and cementation. This sequence is generally similar to that in the other cores from the TAG mound, but clear evidence for two stages of brecciation and cementation are present in cores from Hole 957P. The first veins to form in the basalt clasts were early, thin (0.1–1 mm), pyrite veins. These are cut by 1- to 3-mm quartz + pyrite veins and are reopened by 1- to 3-mm, white quartz veins. The breccia matrix, which consists of white quartz plus 0.1- to 1-mm grains and aggregates of pyrite, cuts earlier quartz + pyrite veins (e.g., interval 158-957P-11R-1, Pieces 3–5). Clasts of basalt with this white quartz + pyrite matrix were rebrecciated, rimmed by a 1- to 3-mm layer of pyrite, and then cemented by a later dark gray quartz + pyrite matrix (e.g., interval 158-957P-10R-1, Piece 1–4, and Samples 158-957P-11R-1, Piece 3, and 12R-2, Pieces 4, 6, and 8). This later dark gray quartz + pyrite matrix is cut by 0.1- to 1-mm vuggy pyrite veins and by 0.5- to 1-cm massive pyrite veins, with late chalcopyrite in open spaces of the pyrite veins (e.g., Sample 158-957P-11R-3, Pieces 7 and 9). Finally, anhydrite occurs on the outer, broken surfaces of many pieces, and fills pore spaces in pyrite veins.

## PHYSICAL PROPERTIES

### Introduction

Physical properties measurements were made on rock samples in cores recovered from Holes 957O and 957P on the northern side of the Black Smoker Complex. Depending on the material available (minicores or fragments), an effort was made to sample representative lithologies for each section recovered. Results are presented according to the type of measurements made for each hole.

### Hole 957O

Physical properties measurements were made on two minicore samples selected as representative from two of the four cores that recovered predominantly pyrite-rich breccias at Hole 957O. Core 158-957O-1R had no recovery and another core (158-957O-3R) recovered only a few pieces that were unsuitable for physical properties measurements.

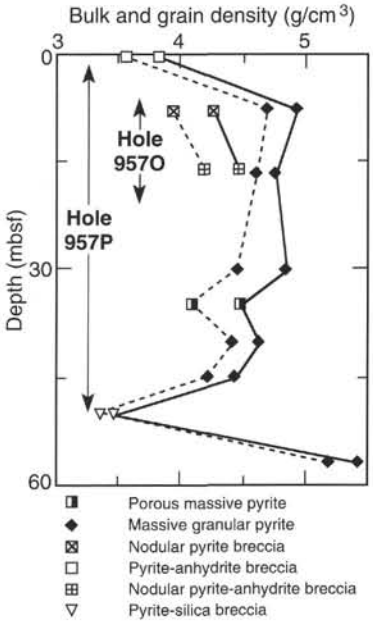


Figure 16. Bulk (dashed line) and grain (solid line) density values of samples identified by rock type vs. depth, Holes 957O and 957P.

#### *Index Properties*

Minicore Sample 158-957O-2R-1, 34–36 cm, extracted from a nodular pyrite breccia, and minicore Sample 158-957O-4R-1, 29–31 cm, extracted from a nodular pyrite-anhydrite breccia, have bulk densities of 4.05 and 4.27 g/cm$^3$ and relatively high porosities of 10.2% and 7.8%, respectively (Table 4, Figs. 16–17).

The two minicores samples (158-957O-2R-1, 34–36 cm, and 4R-1, 29–31 cm) exhibit compressional (*P*-wave) velocities of 5.4 and 5.8 km/s, respectively (Table 5).

The same two minicore samples exhibit resistivities of 0.13 and 0.19 Ωm, respectively (Table 5). The lower resistivity in Sample 158-957O-2R-1, 34–36 cm, is attributed to its higher porosity of 10.2% vs. 7.8% for Sample 158-957O-4R-1, 29–31 cm (Table 5, Fig. 17).

Two half-round samples (158-957O-2R-1, 30–40 cm, Piece 7, and 4R-1, 23–34 cm, Piece 6) from the archive halves of Cores 158-

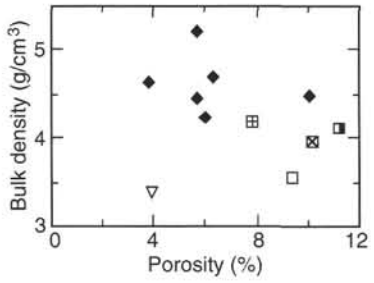


Figure 17. Bulk density vs. porosity for samples identified by rock type, TAG-5 Holes 957O and 957P. Symbols as in Figure 16.

957O-2R and 4R, corresponding to the working halves of the core where the two minicore samples (158-957O-2R-1, 34–36 cm, and 4R-1, 29–31 cm) were extracted, exhibit thermal conductivities (mean of five measurements each) of 10.48 and 10.15 W/(m·K), respectively (Table 6). These values are consistent with measurements made on similar rock types recovered at the TAG-2 area.

## Hole 957P

Physical properties measurements were made using multisensor Track (MST) scanning of two sections of sulfide-rich drill cuttings from Core 158-957P-12R. Index properties were measured on nine fragmentary samples selected as representative from nine of the twelve cores in Hole 957P that were suitable for physical properties measurements.

### *Multisensor Track*

A cumulative length of 1.62 m of drill cuttings comprising Sections 158-957P-12R-1 and 12R-2 was sufficiently intact for multisensor track (MST) measurements, as shown in Figure 18. As the recovered material filled the core liner, no correction for the raw data of wet bulk density measurements by the MST GRAPE device was necessary. Wet bulk densities generally show a narrow range of 2.8 to 3.3 g/cm$^3$ and a slightly increasing trend with depth (Fig. 18). The range of values (6.5–9 cps) for natural gamma radiation throughout both sections of Core 158-957P-12R is small (Fig. 18). The values for volume magnetic susceptibility show a decrease in values from 1200 to 700 $\times$ 10$^{-5}$ SI within Section 158-957P-12R-1, whereas the remaining sections of Core 158-957P-12R show a narrower range of 300–500 $\times$ 10$^{-5}$ SI (Fig. 18) and indicate high concentrations of Fe-oxides.

### *Index Properties*

Index properties for seven of the nine samples measured exhibit relatively high values of bulk densities (4.09–5.19 g/cm$^3$; Table 4 and Fig. 16). The uppermost sample (from 0.4 mbsf) which is classified as a pyrite-anhydrite breccia (Sample 158-957O-1R-1, 38–40 cm), had a lower density of 3.68 g/cm$^3$ and a porosity of 9.4%. The sample recovered from the greatest depth (57 mbsf) had a density of 5.19 g/cm$^3$ and a porosity of 5.7%, as a result of its being comprised of pyrite clasts (Fig. 16). Figure 17 shows the relationship of bulk density vs. porosity. As in the TAG-1 and TAG-2 areas, no clear trend is apparent in these data. Even within a single rock type (i.e., massive granular pyrite, the most common sulfide type recovered from Hole 957P), only a weak inverse correlation between bulk density and porosity is evident (Fig. 17).

## Summary

Eleven sulfide specimens analyzed from the TAG-5 area (Holes 957O and 957P) yielded a range of bulk densities (3.37–5.19 g/cm$^3$) and porosities (3.8%–11.2%) similar to the values measured at the TAG-1 and TAG-2 areas, with no consistent correlation between bulk density and porosity of the different sample types or between these parameters and depth below seafloor. Compressional (*P*-wave) velocities measured on the same minicores are 5.4 and 5.8 km/s. Thermal conductivities measured on half-round slabs are relatively high (10.2 and 10.5 W/[m·K]) and comparable to similar measurements made on cores from the eastern side of the mound.

# PALEOMAGNETISM

At Hole 957O in the TAG 5 area, which is located about 30 m northeast of the Black Smoker Complex, paleomagnetic results were obtained from two minicore samples taken from Sections 158-957O-2R-1 and 4R-1, respectively. Based on our experience with the massive pyrites from the TAG-1 and TAG-2 areas, we first measured the NRM intensity and direction, the initial volume magnetic susceptibility, and the Koenigsberger ratio of the samples. Then we stepwise demagnetized both samples at peak fields of 5, 10, 15, 20, 25, and 30 mT in an effort to remove the soft viscous component of magnetization before the anisotropy of magnetic susceptibility (AMS) of the sample was measured. Finally, both samples were demagnetized in progressive steps of increasing AF field (up to 60 mT) to isolate various magnetic components that may be present. Figure 19 illustrates the magnetic behavior of these samples during AF demagnetization, and Table 7 summarizes their magnetic properties.

**Table 5. Electrical resistance, *P*-wave velocity, and related properties measured in minicores recovered from Hole 957O.**

| Core, section, interval (cm) | Depth (mbsf) | Length (mm) | Diameter (mm) | Resistance (Ω) | Resistivity (Ωm) | Formation factor | *P*-wave velocity (km/s) | Rock type |
|---|---|---|---|---|---|---|---|---|
| 158-957O- | | | | | | | | |
| 2R-1, 34–36 | 8.24 | 24.00 | 25.27 | 6.20 | 0.130 | 0.648 | 5.356 | Nodular pyrite breccia |
| 4R-1, 29–31 | 16.19 | 24.33 | 25.34 | 9.20 | 0.191 | 0.954 | 5.807 | Nodular pyrite-anhydrite breccia |

**Table 6. Thermal conductivity values measured on half-round sulfide samples from Hole 957O.**

| Core, section, interval (cm) | Piece no. | Depth (mbsf) | Thermal conductivity (W/[m·K]) | Error (W/[m·K]) | Rock type |
|---|---|---|---|---|---|
| 158-957O- | | | | | |
| 2R-1, 30–40 | 7 | 8.24 | 10.48 | 0.012 | Nodular pyrite breccia |
| 4 R-1, 23–34 | 6 | 16.19 | 10.15 | 0.013 | Nodular pyrite-anhydrite breccia |

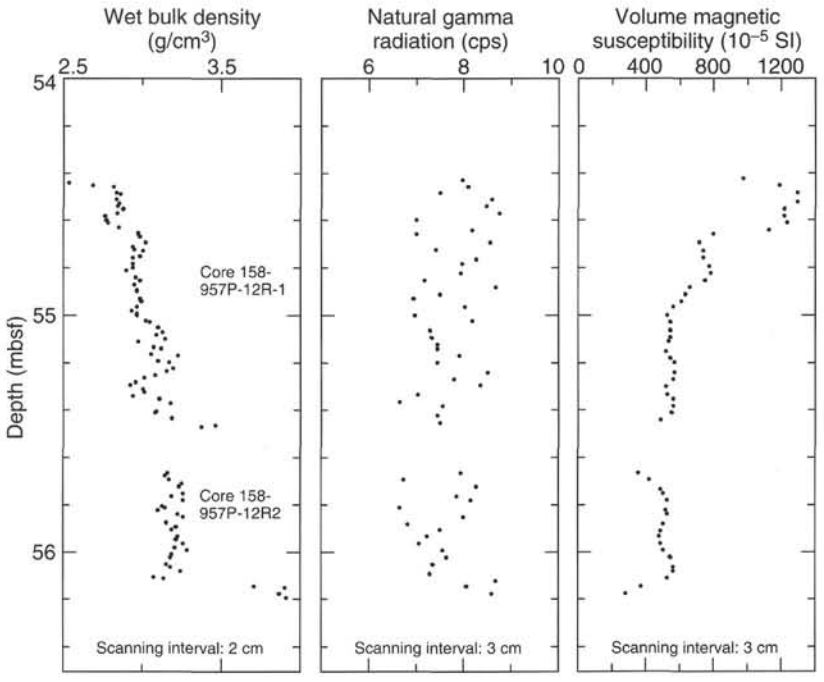


Figure 18. Results from multisensor track (MST) scans of intact intervals of drill cuttings from Core 158-957P-12R (Intervals 158-957P-12R-1, 0–107 cm, and 12R-2, 0–55 cm). The measured physical properties are wet bulk density obtained by the GRAPE instrument, natural gamma radiation, and volume magnetic susceptibility.

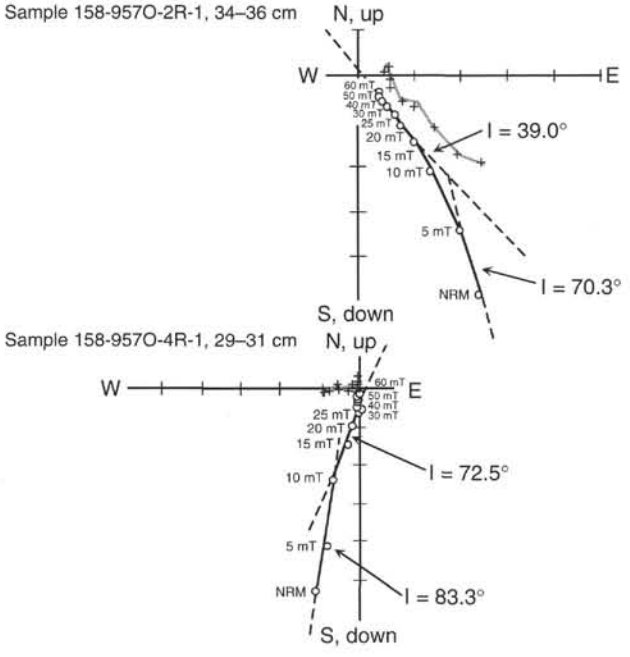


Figure 19. Vector endpoint diagram showing the results of alternating-field demagnetization for discrete samples from Cores 158-957O-2R and 4R. The magnetic component is shown by a straight dashed line fitting the data points, and the corresponding inclination (I) is indicated. Open circles and crosses represent vector endpoints projected onto the vertical and horizontal planes, respectively.

The NRM intensities of Sections 158-957O-2R-1 and 4R-1 are comparable with those of samples recovered from the TAG-1 and TAG-2 areas (on the same order of magnitude). The Koenigsberger ratio and the initial magnetic susceptibility of these two samples, on the other hand, are higher than those of samples taken from the TAG-1 and TAG-2 areas. The anisotropy of magnetic susceptibility (AMS) results from these two pyrite-rich samples are similar to those of samples recovered from the TAG-1 and TAG-2 areas as well as the basalt samples from the TAG-4 area, suggesting that no significant magnetic anisotropy is present in these samples. Both samples exhibited signs of vertically directed, drilling-induced magnetization, as evidenced by the first component of magnetization during initial demagnetization (Fig. 19). This component has almost vertical inclination and can be removed relative easily from the nodular pyrite breccia (Sample 158-957O-2R-1, 34–36 cm). In the nodular pyrite-anhydrite breccia (Sample 158-957O-4R-1, 29–31 cm), however, AF demagnetization is not sufficient to remove this overprint completely. As shown in Figure 20, the demagnetization path for Sample 158-957O-4R-1, 29–31 cm, corresponds to a great circle diverging from a initially steeply inclined, downward magnetization. The large deviation from the expected direction (I = 55) observed in the data results from incomplete removal of the drilling-induced remagnetization. Similar examples of this behavior are also seen in samples from other TAG areas (see "Paleomagnetism" sections, Chapters 7 and 8, this volume). It appears that the more heavily overprinted samples are often associated with the presence of anhydrite (e.g., pyrite-anhydrite-breccia) and also come from relatively deeper sections in the mound. This information leads us to suspect that the pervasive hydrothermal activity that has affected the entire TAG mound may have produced distinct zones where rocks have their own characteristic magnetic properties. These zones are likely to reflect different mineralogical and chemical compositions and, therefore, a variable ability to acquire and maintain magnetic overprints. This hypothesis can be tested by a combined study of mineralogical examinations and rock magnetic experiments.

**Table 7. Magnetic properties of minicore samples from Hole 957O.**

| Core, section, interval (cm) | Depth (mbsf) | NRM intensity (mA/m) | Declination (degrees) | Inclination (degrees) | K ($10^{-6}$ SI) | Q ratio | $P = K_1/K_3$ |
|---|---|---|---|---|---|---|---|
| 158-957O- | | | | | | | |
| 2R-1, 34–36 | 8.24 | 14.90 | 140.0 | 39.0 | 72.67 | 6.131 | 1.035 |
| 4R-1, 29–31 | 16.19 | 27.50 | 261.2 | 72.5 | 109.0 | 7.545 | 1.041 |

Notes: Inclination = stable inclination after demagnetization; K = magnetic susceptibility in $10^{-6}$ SI units; Q ratio = Koenigsberger ratio; P = anisotropy factor; and $K_1$ and $K_3$ = maximum and minimum principal axes of susceptibility.

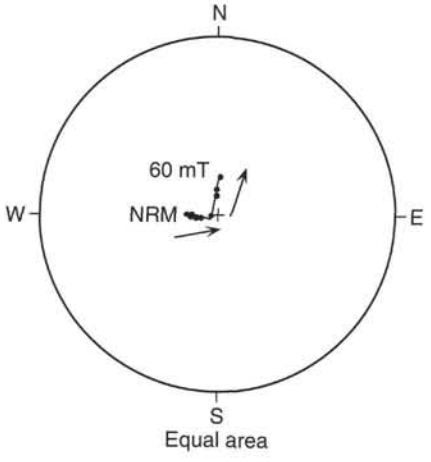


Figure 20. Equal-area projection of the directional variations observed in Sample 158-957O-4R-1, 29–31 cm, during AF demagnetization. The demagnetization path corresponds to a great circle that diverges from an initially steeply inclined magnetization. The large deviation from the expected inclination observed in the data suggests incomplete removal of the drilling-induced overprint.

## REFERENCE

Tivey, M.K., Humphris, S.E., Thompson, G., Hannington, M.D., and Rona, P.A., 1995. Deducing patterns of fluid flow and mixing within the TAG active hydrothermal mound using mineralogical and geochemical data. *J. Geophys. Res.*, 100:12527–12555.

**Ms 158IR-111**

**NOTE: For all sites drilled, core-description forms ("barrel sheets") and core photographs can be found in Section 3, beginning on page 227. Thin-section data are given in Section 4, beginning on page 345.**